

LA-UR-15-20009 (Accepted Manuscript)

Fast magnetic reconnection with large guide fields

Stanier, Adam John
Simakov, Andrei Nikolaevich
Chacon, Luis
Daughton, William Scott

Provided by the author(s) and the Los Alamos National Laboratory (2016-07-14).

To be published in: Physics of Plasmas

DOI to publisher's version: 10.1063/1.4905629

Permalink to record: <http://permalink.lanl.gov/object/view?what=info:lanl-repo/lareport/LA-UR-15-20009>

Disclaimer:

Approved for public release. Los Alamos National Laboratory, an affirmative action/equal opportunity employer, is operated by the Los Alamos National Security, LLC for the National Nuclear Security Administration of the U.S. Department of Energy under contract DE-AC52-06NA25396. Los Alamos National Laboratory strongly supports academic freedom and a researcher's right to publish; as an institution, however, the Laboratory does not endorse the viewpoint of a publication or guarantee its technical correctness.



Fast magnetic reconnection with large guide fields

A. Stanier, Andrei N. Simakov, L. Chacón, and W. Daughton

Version of Record Citation: [Physics of Plasmas](#) **22**, 010701 (2015); doi: 10.1063/1.4905629

View Version of Record online: <http://dx.doi.org/10.1063/1.4905629>

View Table of Contents: <http://scitation.aip.org/content/aip/journal/pop/22/1?ver=pdfcov>

Publisher: [AIP Publishing](#)

Articles you may be interested in

[Fast magnetic reconnection due to anisotropic electron pressure](#)

Phys. Plasmas **22**, 020705 (2015); 10.1063/1.4908545

[The effect of guide-field and boundary conditions on collisionless magnetic reconnection in a stressed X-point collapse](#)

Phys. Plasmas **21**, 012901 (2014); 10.1063/1.4861258

[The Hall fields and fast magnetic reconnection](#)

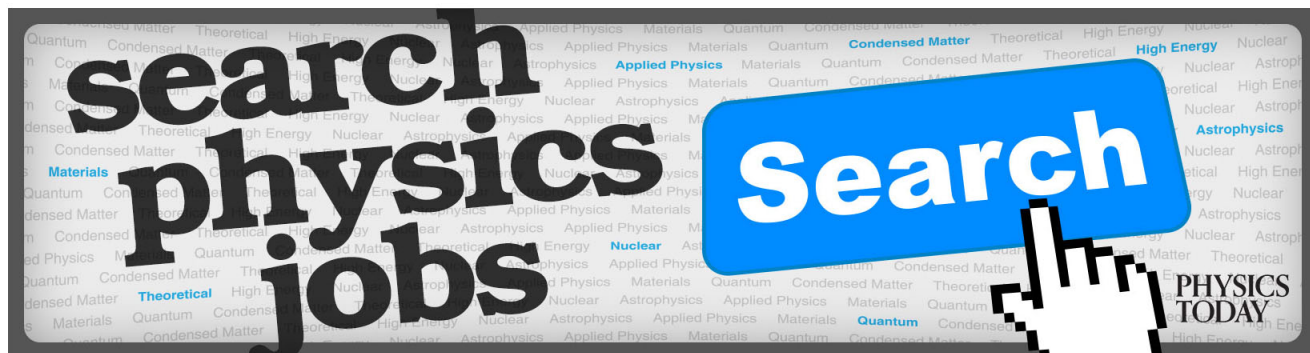
Phys. Plasmas **15**, 042306 (2008); 10.1063/1.2901194

[Electron acceleration during guide field magnetic reconnection](#)

Phys. Plasmas **15**, 032903 (2008); 10.1063/1.2876465

[Catastrophic onset of fast magnetic reconnection with a guide field](#)

Phys. Plasmas **14**, 054502 (2007); 10.1063/1.2734948



Fast magnetic reconnection with large guide fields

A. Stanier,^{1, a)} Andrei N. Simakov,¹ L. Chacón,¹ and W. Daughton¹
 Los Alamos National Laboratory, Los Alamos, New Mexico 87545, USA

(Dated: 11 December 2014)

In this Letter, it is demonstrated using two-fluid simulations that low- β magnetic reconnection remains fast, regardless of the presence of fast dispersive waves, which have been previously suggested to play a critical role. To understand these results, a discrete model is constructed that offers scaling relationships for the reconnection rate and dissipation region (DR) thickness in terms of the upstream magnetic field and DR length. We verify these scalings numerically, and show how the DR self-adjusts to process magnetic flux at the same rate that it is supplied to a larger region where two-fluid effects become important. The rate is therefore independent of the DR physics, and is in good agreement with kinetic results.

Magnetic reconnection is the changing of magnetic field-line connectivity within highly conducting plasmas by localised magnetic flux unfreezing. Low- β reconnection, where the magnetic field is dominated by a strong *guide* component $B_0\hat{z}$, is the regime pertinent to laboratory magnetic confinement devices,^{1–5} the solar corona,⁶ and other magnetically dominated astrophysical environments. Despite the importance of these applications, low- β reconnection remains poorly understood.

An outstanding theoretical question concerns the fast timescales of reconnection in nature, compared to collisional timescales. Numerical and analytic models^{7–11} have shown that low- β reconnection can be fast, independent of collisional dissipation and system-size, when the collisional dissipation region (DR) thickness, δ , falls below the sound-Larmor radius $\rho_s = \sqrt{T_e/m_i}/\Omega_{ci}$. Here, T_e is the electron temperature, m_i the ion mass, $\Omega_{ci} = qB_0/m_i$ the ion-cyclotron frequency, and q the ion charge.

While there is still no rigorous theory, it has been suggested¹⁰ that fast-dispersive waves (FDWs), with frequency $\omega \propto k^2$ for wavenumber k , play a critical role in facilitating fast reconnection. However, recent low- β kinetic simulations^{12,13} have demonstrated that reconnection remains fast even in the absence of FDWs. Fast-reconnection can also occur in pair-plasmas that do not support such waves,^{14–16} and in the single-fluid limit with non-uniform dissipation.^{17,18} Finally, in time-dependent studies, faster than exponential tearing growth-rates have been demonstrated in the non-linear regime when finite electron inertia,¹⁹ or finite ion gyro-radius,^{20–22} effects are included.

In this Letter, we show that low- β reconnection is formally fast (Alfvénic, and independent of collisional dissipation and system-size) for both $\rho_s > d_e$ (case with FDWs) and $\rho_s \leq d_e$ (no FDW case), where $d_e = c/\omega_{pe}$ is the electron skin-depth, c the speed of light, and ω_{pe} the electron plasma frequency. To understand why reconnection is fast in both cases, we perform a quasi steady-state analysis of the DR and its coupling to the surrounding region where two-fluid effects are important. This analysis

offers scaling relationships for the DR thickness and reconnection rate in terms of the upstream magnetic field and the DR length. It is an extension of previous discrete DR models in electron MHD,^{23,24} Hall-MHD,^{25,26} pair-plasmas,¹⁶ and a low- β regime with resistive DRs and finite- ρ_s .¹¹ The scalings we obtain are carefully verified by two-fluid simulations, and related to the magnetic field and length of a surrounding region in which two-fluid effects become important. For both cases, the DR self-adjusts to permit reconnection at the rate set by the inflow of flux into this larger region of thickness $h = \max[\rho_s, d_e]$. Specifically, the DR maintains a constant aspect-ratio when $\delta < \rho_s$, and the upstream magnetic field $B_x \propto \delta$ when $\delta < h$. The resultant rates are independent of the DR physics, so that two-fluid simulations can reproduce the fast-reconnection observed in kinetic simulations.^{12,13,27}

Two-field model. The low- β , two-field reconnection equations,^{7–9,11,28,29} normalised by a characteristic Alfvén velocity and macroscopic length-scale, are

$$(\partial_t + \mathbf{v} \cdot \nabla)\omega = \mathbf{B} \cdot \nabla j + \mu \nabla^2 \omega, \quad (1)$$

$$\begin{aligned} \partial_t \mathbf{B}^* - \nabla \times (\mathbf{v} \times \mathbf{B}^*) &= \rho_s^2 \nabla \times [\mathbf{B} \times (\hat{z} \times \nabla \omega)] \\ &- \nabla \times [\nabla \times (\eta \mathbf{B} - \eta_H \nabla^2 \mathbf{B})], \end{aligned} \quad (2)$$

where $\mathbf{B} = \hat{z} \times \nabla \psi$ is the in-plane magnetic field with magnetic flux ψ , $\mathbf{v} = \hat{z} \times \nabla \phi$ the in-plane velocity with stream-function ϕ , $\omega = \hat{z} \cdot \nabla \times \mathbf{v}$ the vorticity, $j = \hat{z} \cdot \nabla \times \mathbf{B}$ the out-of-plane current density, and $\mathbf{B}^* = \mathbf{B} + d_e^2 \nabla \times (\nabla \times \mathbf{B})$. Also, μ is the ion collisional viscosity, η the plasma resistivity, and $\eta_H = d_i^2 \mu_e$ the hyper-resistivity with $d_i = \sqrt{m_i/m_e} d_e$ the ion-skin depth, and μ_e the electron collisional viscosity.³⁰ When $d_e = \eta = \eta_H = 0$, Eq. (2) becomes $\partial_t \psi + \mathbf{v}_s \cdot \nabla \psi = 0$, where $\mathbf{v}_s = \hat{z} \times \nabla (\phi - \rho_s^2 \nabla^2 \phi)$ is the velocity that carries the frozen-in magnetic flux.^{9,31} Physically, this is an electron perpendicular velocity that combines the $\mathbf{E} \times \mathbf{B}$ and diamagnetic drifts.

In a uniform collisionless ($\eta = \mu = \eta_H = 0$) plasma, Eqs. (1,2) support waves with dispersion relation

$$\omega = k_{\parallel} \sqrt{(1 + \rho_s^2 k^2)/(1 + d_e^2 k^2)}, \quad (3)$$

where $k_{\parallel} = \hat{\mathbf{b}}_0 \cdot \mathbf{k}$, and $\hat{\mathbf{b}}_0$ is the unit vector along the magnetic field. In the limit $\rho_s^2 k^2 \gg 1 \gg d_e^2 k^2$, Eq. (3)

^{a)}Electronic mail: stanier@lanl.gov

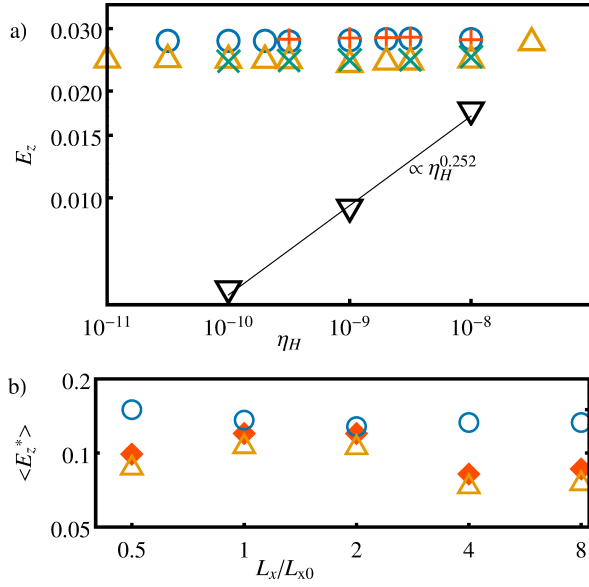


FIG. 1. a) Peak rates in island coalescence runs. b) Normalised rates against system-size (L_x/L_{x0} , where $L_{x0} = 100h$) from fluid (uniform $\eta_H = 10^{-9}$) and PIC Harris-sheet simulations. Fluid simulations are: $d_e = \rho_s = 0$ (black ∇); $d_e = 5\rho_s = 10^{-2}$ (orange \triangle); $d_e = 10^{-2}$, $\rho_s = 0$ (green \times); $\rho_s = 5d_e = 10^{-2}$ (blue \circ); and $\rho_s = 10^{-2}$, $d_e = 0$ (red $+$). The PIC runs have $d_e = 5\rho_s = 10^{-2}$ (red \blacklozenge).

describes the fast-dispersive kinetic Alfvén wave with $\omega = \rho_s k_{\parallel} k$. However, for $\rho_s \leq d_e$ there are no FDWs.

Numerical results. We solved Eqs. (1, 2) numerically with the low- β formulation³² of the PIXIE2D code,^{33,34} for the island coalescence and Harris sheet reconnection problems. The island coalescence calculations were solved in a quarter domain $[0, 1] \times [0, 1]$ with initial conditions identical to those in Ref. 35. The fluid Harris-sheet runs used a half-domain $[-L_x, L_x] \times [0, 0.5]$ with equilibrium current-sheet thickness $\lambda = 1/(8\pi) \approx 4h$, and initiated with a 3% perturbation of the upstream field strength. The Harris sheet runs were also compared with fully kinetic particle-in-cell (PIC) simulations using the VPIC code,³⁶ with the same fluid-scale parameters³⁷ and initial conditions. For the fluid simulations, we focus on viscous DRs ($\eta = 0$; $\eta_H, \mu \neq 0$), as resistivity alone can not prevent DR collapse for $\delta < h$.^{11,24} The ratio of ion viscosity to hyper-resistivity is set at $\mu/\eta_H = 10^4$, which provides sufficient dissipation in Eq. (1) to prevent numerical instability, while remaining close to the inviscid limit (several simulations were repeated for $\mu \rightarrow 0$, with results largely unchanged). The precise value of μ/η_H chosen does not affect our conclusions.

Figure 1a shows the dependence of the peak reconnection rate, $E_z = \partial_t \psi|_X$ evaluated at the X-point and normalised to the Alfvénic rate on the edge of the domain, on collisional dissipation, η_H , from a series of island-coalescence simulations. Shown are two-fluid cases without FDWs (orange \triangle and green \times), with FDWs (blue \circ and red $+$), and the single-fluid case (black ∇).

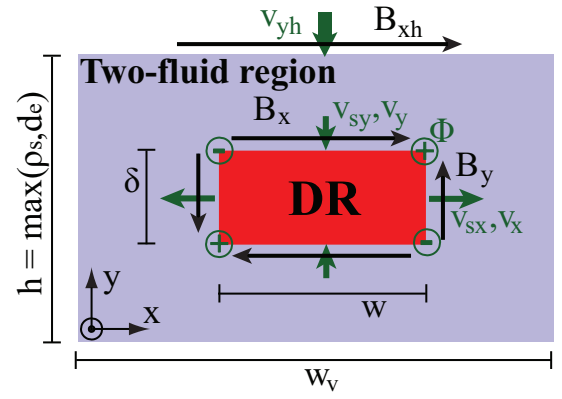


FIG. 2. Schematic of the reconnection region geometry. The dissipation region (DR, red) is defined with thickness δ , which depends on collisional dissipation, and length w , set by the extent of flux carrying outflow jets v_{sx} . This is embedded in a larger two-fluid region (purple) defined with thickness $h = \max(\rho_s, d_e)$, and length w_v set by the extent of single-fluid outflow jets v_x .

The single-fluid rate with uniform η_H is formally slow (dissipation dependent) as $E_z \propto \eta_H^{0.252}$. However, in all two-fluid cases the rate becomes dissipation independent when δ falls below h ; as η_H is reduced the DR thickness δ decreases, and we find that $\delta \lesssim h$ for $\eta_H \lesssim 10^{-8}$ in these simulations. In these runs, the rates are also independent of the smallest two-fluid scale, $p = \min[\rho_s, d_e]$, as they are the same for $p = 0$ (green \times and red $+$) and for $p \neq 0$ (orange \triangle and blue \circ), even when δ falls below p (which occurs for $\eta_H \lesssim 10^{-9.5}$). We note that the reconnection rate obtained for Harris-sheet simulations in runs without significant secondary island formation is also independent of η_H when $\delta \ll h$ (not shown).

Figure 1b shows the variation of the normalised peak reconnection rate $\langle E_z^* \rangle$ with system-size (L_x/L_{x0} , where $L_{x0} = 100h$) from fluid and PIC Harris-sheet simulations. Here

$$\langle E_z^* \rangle = \frac{1}{(\hat{x} \cdot \mathbf{v}_A)(\hat{x} \cdot \mathbf{B})} \left\langle \frac{\partial \psi_r}{\partial t} \right\rangle, \quad (4)$$

where $\psi_r = \max(\psi) - \min(\psi)$ is the flux difference between dominant X and O-points, $\langle \rangle$ is an average over the time required for an Alfvén wave to cross the whole box in the inflow direction, and $(\hat{x} \cdot \mathbf{v}_A)(\hat{x} \cdot \mathbf{B})$ is the Alfvén rate at $4h$ upstream of the main X-point.³⁸ Despite a factor of 16 change in L_x , there is no appreciable variation in $\langle E_z^* \rangle$ for cases with or without FDWs. Also, for the case without FDWs, fluid rates closely follow the PIC rates, implying that Eqs. (1, 2) contain sufficient physics to reproduce the fast rates recently demonstrated in kinetic simulations without FDWs.^{12,13} Note that $\langle E_z^* \rangle$ is a significant fraction of an Alfvénic rate in both cases, with and without FDWs, so that both cases satisfy all criteria for fast-reconnection: the rate is Alfvénic, independent of dissipation and of system-size.

Analytic model. To construct the analytic model, Eqs. (1, 2) are discretised at a DR of thickness δ and length w , as shown in Fig. 2, using the technique of Refs. 11, 16, and 23. The discrete magnetic field components are $B_x = \hat{x} \cdot \mathbf{B}(0, \delta/2)$, $B_y = \hat{y} \cdot \mathbf{B}(w/2, 0)$, and the discrete single-fluid velocities are $v_y = -2\Phi/w$ and $v_x = 2\Phi/\delta$, defined with the discrete flow stream function $\Phi = -\phi(w/2, \delta/2)$. We focus on quasi-steady behaviour, where time derivatives are small and can be neglected. This is often a good approximation when the system reaches non-linear saturation, such as at the time of peak reconnection rate in the island-coalescence problem.³⁹ Neglecting numerical factors of order unity gives three equations that can be solved parametrically for five unknowns ($\delta, w, B_x, B_y, \Phi$)

$$\frac{\Phi^2}{\delta w} \left(\frac{1}{\delta^2} - \frac{1}{w^2} \right) + \left(\frac{B_x}{w} + \frac{B_y}{\delta} \right) \left(\frac{B_y}{w} - \frac{B_x}{\delta} \right) = -\mu \Phi \Delta^2, \quad (5)$$

$$-\frac{\Phi}{\delta w} \left[B_x (1 + \rho_s^2 \Delta) - d_e^2 \left(\frac{B_y}{\delta w} - \frac{B_x}{\delta^2} \right) \right] = D \left(\frac{B_y}{\delta w} - \frac{B_x}{\delta^2} \right), \quad (6)$$

$$\frac{\Phi}{\delta w} \left[B_y (1 + \rho_s^2 \Delta) - d_e^2 \left(\frac{B_x}{\delta w} - \frac{B_y}{w^2} \right) \right] = D \left(\frac{B_x}{\delta w} - \frac{B_y}{w^2} \right), \quad (7)$$

where $D = \eta + \eta_H \Delta$, and $\Delta = \delta^{-2} + w^{-2}$. This set of discrete equations combine the finite- ρ_s terms of Ref. 11 and the finite- d_e terms of Ref. 16.

To simplify Eqs. (5-7), we assume that the aspect-ratio δ/w is small, such that the approximation $1 + \delta^2/w^2 \approx 1 - \delta^2/w^2 \approx 1$ is valid. It is also assumed that the DR length is large enough such that $w^2/d_e^2 \gg 1$. Both of these assumptions are motivated by the numerical simulations used in Fig. 1, where they are well satisfied. Finally, as in the simulations, we set $\eta = 0$.

Eliminating Φ and B_y gives an equation for $\delta(B_x, w)$,

$$\frac{\delta^4}{w^8} \frac{(\delta^2 + \rho_s^2 + d_e^2)^3}{\delta^2 + \rho_s^2} = \frac{1}{S_H^2} \left[1 + \frac{\mu(\delta^2 + \rho_s^2 + d_e^2)}{\eta_H} \right], \quad (8)$$

where $S_H \equiv \sqrt{2} B_x w^3 / \eta_H$ is the hyper-resistive Lundquist number. The quasi-steady ($\partial_t j = 0$) reconnection rate is then

$$E_z \approx D \left(\frac{B_x}{\delta} - \frac{B_y}{w} \right) \approx \eta_H B_x / \delta^3. \quad (9)$$

Single-fluid case ($\delta^2 \gg \max[\rho_s^2, d_e^2]$). Assuming $\mu = 0$, and using Eqs. (8,9) gives the well-known scalings⁴⁰

$$\delta = \delta_H \equiv w S_H^{-1/4}, \quad E_z = E_{zH} \equiv \sqrt{2} B_x^2 S_H^{-1/4}. \quad (10)$$

From numerical simulations, the DR length w is a macroscopic length-scale that corresponds to the distance between maxima of the ion outflow jets. For $\mu \neq 0$ two limiting cases are possible. When $\sqrt{S_H}/S_\mu \ll 1$, where $S_\mu = \sqrt{2} B_x w / \mu$ is the viscous Lundquist number, the rate

has a small correction $E_z \approx E_{zH} (1 - 3\sqrt{S_H}/8S_\mu)$, but for $\sqrt{S_H}/S_\mu \gg 1$ the rate can be significantly reduced $E_z = E_{zH} S_\mu^{1/2} S_H^{-1/4}$. The rate $E_z \propto S_H^{-1/4}$ is shown in Fig. 1a (black inverted triangles), where $B_x, w \propto \eta_H^0$.

Two-fluid case without FDWs ($d_e^2 \gg \rho_s^2, \delta^2$). In what follows, we assume for simplicity that the ratio of ion to electron viscosity is fixed to the simulation value, $\mu/\eta_H = 1/(\rho_s^2 + d_e^2) \approx 10^4$, and discuss the effect of varying ion viscosity below. We consider two limiting cases: for $d_e^2 \gg \delta^2 \gg \rho_s^2$, Eqs. (8,9) give $\delta = w \eta_H / (B_x d_e^3)$, and $E_z = B_x^4 d_e^9 / (\eta_H^2 w^3)$; for $d_e^2 \gg \rho_s^2 \gg \delta^2$ we get $\delta = [w \eta_H \rho_s / (B_x d_e^3)]^{1/2}$ and $E_z = [B_x^5 d_e^9 / (\eta_H \rho_s^3 w^3)]^{1/2}$. In both limits, the rate appears to be ‘‘super-fast’’, that is $E_z \propto \eta_H^\alpha$ with $\alpha < 0$. This is unphysical and contradicts the numerical results in Fig. 1a, where $E_z \propto \eta_H^0$ across both the $d_e^2 \gg \delta^2 \gg \rho_s^2$ (orange Δ for $10^{-8} \geq \eta_H > 10^{-9.5}$, and green \times) and $d_e^2 \gg \rho_s^2 \gg \delta^2$ (orange Δ with $\eta_H \leq 10^{-9.5}$) limits. This apparent contradiction is resolved as the two free-parameters in the discrete model, B_x and w , scale with η_H to give $E_z \propto \eta_H^0$ as seen in simulations.

The first limit, $d_e^2 \gg \delta^2 \gg \rho_s^2$, is fully analogous to the low- β pair-plasma case.¹⁶ As in Ref. 16, our numerical simulations show that the bulk of the current-layer is supported at d_e -scale, which is also consistent with kinetic simulations.¹² At smaller scales the plasma becomes demagnetised, and the magnetic field on the upstream edge of the DR scales as $B_x = (\delta/d_e) B_{xd}$ with $B_{xd} = \hat{x} \cdot \mathbf{B}(0, d_e/2)$. This gives a rate not explicitly dependent upon η_H , provided $w \propto \eta_H^0$. We see in these island coalescence simulations that $w = w_v \propto \eta_H^0$ in this limit, where w_v is on the order of the island size. Using this B_x scaling in the second limit, $d_e^2 \gg \rho_s^2 \gg \delta^2$, the DR length w must scale to ensure fixed aspect-ratio as $\delta/w = \rho_s/w_v$ for the rate to remain constant across the two limits. These scalings for B_x and w are verified numerically, as discussed below. The resulting DR thickness and rate for the two-fluid case without FDWs are

$$\delta = \frac{\delta_d^2}{d_e}, \quad E_z = B_{xd}^2 \frac{d_e}{w_v}, \quad (11)$$

where $\delta_d = w_v (\eta_H / B_{xd} w_v^3)^{1/4}$ is equal to the single-fluid thickness in Eq. (10), evaluated with B_{xd} and w_v (at the boundary of the two-fluid region, see Fig. 2).

Two-fluid case with FDWs ($\rho_s^2 \gg d_e^2, \delta^2$). We again consider two limiting cases, $\rho_s^2 \gg d_e^2 \gg \delta^2$ and $\rho_s^2 \gg \delta^2 \gg d_e^2$. In both limits, Eqs. (8,9) give $\delta = [\eta_H w / (B_x \rho_s^2)]^{1/2}$ and $E_z = [B_x^5 \rho_s^6 / (\eta_H w^3)]^{1/2}$, where the rate again appears to be super-fast for $B_x, w \propto \eta_H^0$. In the first limit, $\delta < d_e$ and we expect $B_x = (\delta/d_e) B_{xd}$ as before, which requires $w \propto \delta$ to give a rate that is independent of η_H as in the simulations. We show below from numerical simulations that the fixed aspect-ratio scaling ($\delta/w \propto \rho_s/w_v$) occurs whenever $\delta < \rho_s$, regardless of d_e . In the second limit, $\delta > d_e$ and so a B_x scaling is not known *a priori* from physical arguments. However, with $\delta/w \propto \rho_s/w_v$, we must have

$B_x \propto \delta$ to give a constant and fast-rate across both limits. We find for both limits that, to a good approximation, $B_x \approx (\delta/\rho_s)B_{xs}$ with $B_{xs} = \hat{\mathbf{x}} \cdot \mathbf{B}(0, \rho_s/2)$. The DR thickness and rate for the case with FDWs is

$$\delta = \frac{\delta_s^2}{\rho_s}, \quad E_z = B_{xs}^2 \frac{\rho_s}{w_v}, \quad (12)$$

where $\delta_s = w_v(\eta_H/B_{xs}w_v^3)^{1/4}$.

Numerical validation. The scalings for B_x and w are verified using the previously described island coalescence simulations. For each simulation, we measure $(\delta, w, B_x, w_v, B_{xh})$ at peak reconnection rate. The thickness δ is measured in the same way as in Ref. 16, by fitting the current as $j(0, y) = e^{-ay^2/\delta^2}$ with $a = 4 \ln 2$ to give δ as the full-width half-maximum $j(0, \delta/2) = j(0, 0)/2$. Thus, $\delta = \sqrt{2ay^*}$, where y^* is the closest distance to the X-point that $|(\partial_y^2 j)/j|_{(0, y^*)} = 0$. This method does a good job of capturing the thickness of the viscous DR, as discussed in Ref. 16. The lengths w and w_v , shown in Fig. 2, are defined as the distance between the maxima of $\hat{\mathbf{x}} \cdot \mathbf{v}_s|_{y=0}$ and $\hat{\mathbf{x}} \cdot \mathbf{v}|_{y=0}$, respectively. B_x and B_{xh} are evaluated at $(0, \delta/2)$ and $(0, h/2)$ respectively, as shown in Fig. 2.

Figure 3a shows the scalings of w/w_v and w_v with δ/ρ_s in the two-fluid cases without (orange triangles) and with (blue circles and red +) FDWs. There is a clear linear dependence of w/w_v on δ/ρ_s in both cases, validating the scaling for w used in the analysis above. The change of $\approx \sqrt{2}$ in slope between cases with and without FDWs does not appear in the analytic model due to neglecting numerical factors of order unity in the discretisation. The $w \propto \delta$ scaling is a finite- ρ_s effect, and is largely unaffected by d_e -scale physics.

Figure 3b shows the scaling of B_x and B_{xh} with δ/h in both two-fluid cases. The DR parameter B_x decreases linearly with δ/h as required, while the two-fluid parameter B_{xh} is approximately independent of δ . In this plot, B_x is fit with two straight lines for each case, as there is a slope change of ≈ 2 when $\delta = p = h/5$ that is not captured by the analytic model due to neglecting factors of order unity.

As a further validation of the model, Fig. 3c shows the ratio of the measured and predicted DR thicknesses, where δ_{theory} is given in Eqs. (11,12), and demonstrates an overall excellent agreement over almost two orders of magnitude in δ .

The value of μ chosen for the analytic calculations and simulations in this Letter is close to the inviscid limit. Increasing μ gives a thicker DR, and slower outflows, as expected. However, we find in these island coalescence simulations that for moderate increases in μ , such that $\delta < h$ holds, the DR and two-fluid regions self-adapt such that the reconnection rate is largely unaffected. This is in contrast to the single-fluid limit where large ion viscosity can significantly slow the reconnection rate.

Interpretation. From the analytic scalings in both two-fluid cases, the viscous DR has the potential to process flux at a super-fast rate for $B_x, w \propto \eta_H^0$. However, the DR rate can not physically exceed the rate of flux brought

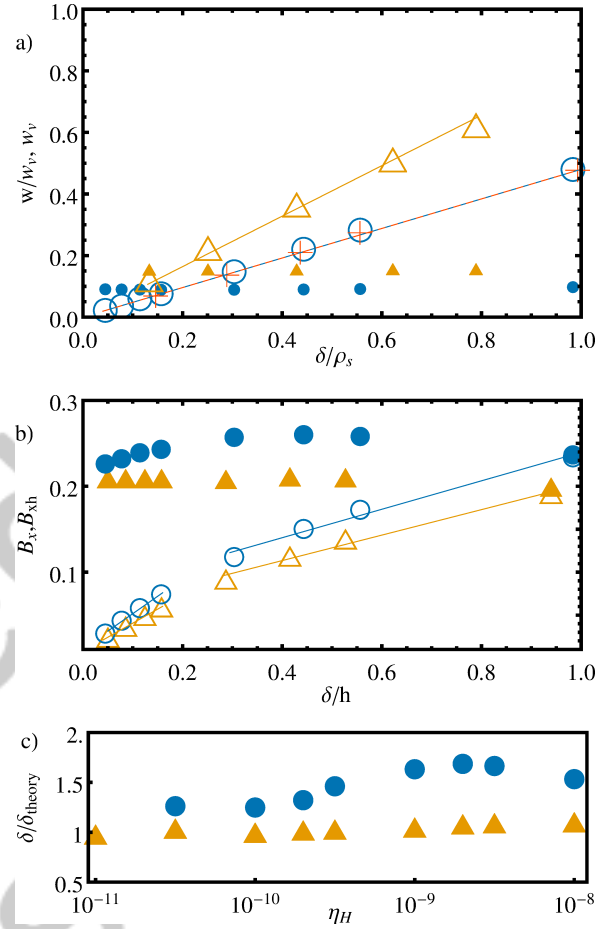


FIG. 3. a) w/w_v (hollow with linear fits) and w_v (filled) against δ/ρ_s ; b) B_x (hollow with linear fits) and B_{xh} (filled) against δ/h ; c) ratio of simulated, δ , to predicted, δ_{theory} from Eqs. (11, 12), DR thicknesses. From island coalescence simulations with $d_e = 5\rho_s = 10^{-2}$ (orange triangles); $\rho_s = 5d_e = 10^{-2}$ (blue circles); and $\rho_s = 10^{-2}$, $d_e = 0$ (red + for w/w_v).

into the larger two-fluid region in Fig. 2. The latter rate is simply given by $v_{yh}B_{xh}$, where $v_{yh} = (h/w_v)B_{xh}$ due to flow continuity with the outflow accelerated to the upstream ion Alfvén speed (B_{xh} in normalised units). The DR self-adjusts to match this upper bound, giving

$$E_z = B_{xh}^2 \frac{h}{w_v}, \quad (13)$$

in both two-fluid cases, where w_v and B_{xh} are shown in Figs. 3a, 3b to be independent of δ (and so η_H). The DR self-adjusts by shrinking in length at constant aspect ratio when finite- ρ_s effects become important, and by regulating the upstream field B_x in the case of either finite- ρ_s or finite- d_e .

This self-adjustment of the DR gives a dissipation independent rate, in agreement with Fig. 1a. A full discussion of the system-size independence in Fig. 1b is beyond the scope of this Letter, and will be addressed in future work. We note that the rates between the cases with and

without FDWs are similar, consistent with Refs. 12 and 13. However, the mechanism to limit $w_v \propto L_x^0$, and give a rate independent of system-size, is not necessarily the same between the two cases. For instance, we see more secondary island formation in the case without FDWs, but it is not clear whether this is the sole mechanism that limits w_v .

ACKNOWLEDGMENTS

This work is supported by the U.S. Department of Energy, Office of Science, and Office of Fusion Energy Sciences, and used resources provided by the Los Alamos National Laboratory Institutional Computing Program, which is supported by the U.S. Department of Energy National Nuclear Security Administration under Contract No. DE-AC52-06NA25396. Contributions from W.D. were supported by NASA through the Heliospheric Theory Program. A.S. would like to thank Yi-Hsin Liu for helpful discussions, and the anonymous referees for their suggestions.

- ¹M. Yamada, F. M. Levinton, N. Pomphrey, R. Budny, J. Manickam, and Y. Nagayama, *Phys. Plasmas* **1**, 3269 (1994).
- ²I. T. Chapman, R. Scannell, W. A. Cooper, J. P. Graves, R. J. Hastie, G. Naylor, and A. Zocco, *Phys. Rev. Lett.* **105**, 255002 (2010).
- ³Y. Ono, H. Tanabe, Y. Hayashi, T. Ii, Y. Narushima, T. Yamada, M. Inomoto, and C. Z. Cheng, *Phys. Rev. Lett.* **107**, 185001 (2011).
- ⁴A. Stanier, P. Browning, M. Gordovskyy, K. G. McClements, M. P. Gryaznevich, and V. S. Lukin, *Phys. Plasmas* **20**, 122302 (2013).
- ⁵P. K. Browning, A. Stanier, G. Ashworth, K. G. McClements, and V. S. Lukin, *Plasma Phys. Control. Fusion* **56**, 064009 (2014).
- ⁶E. Priest and T. Forbes, *Magnetic Reconnection* (Cambridge University Press, Cambridge, Cambridge, 2000).
- ⁷R. G. Kleva, J. F. Drake, and F. L. Waelbroeck, *Phys. Plasmas* **2**, 23 (1995).
- ⁸A. Bhattacharjee, K. Germaschewski, and C. S. Ng, *Phys. Plasmas* **12**, 042305 (2005).
- ⁹S. Schmidt, S. Günter, and K. Lackner, *Phys. Plasmas* **16**, 072302 (2009).
- ¹⁰B. N. Rogers, R. E. Denton, J. F. Drake, and M. A. Shay, *Phys. Rev. Lett.* **87**, 195004 (2001).
- ¹¹A. N. Simakov, L. Chacón, and A. Zocco, *Phys. Plasmas* **17**, 060701 (2010).
- ¹²Y.-H. Liu, W. Daughton, H. Karimabadi, H. Li, and S. P. Gary, *Phys. Plasmas* **21**, 022113 (2014).
- ¹³J. M. TenBarge, W. Daughton, H. Karimabadi, G. G. Howes, and W. Dorland, *Phys. Plasmas* **21**, 020708 (2014).
- ¹⁴N. Bessho and A. Bhattacharjee, *Phys. Rev. Lett.* **95**, 245001 (2005).
- ¹⁵W. Daughton and H. Karimabadi, *Phys. Plasmas* **14**, 072303 (2007).
- ¹⁶L. Chacón, A. N. Simakov, V. S. Lukin, and A. Zocco, *Phys. Rev. Lett.* **101**, 025003 (2008).
- ¹⁷M. Ugai and T. Tsuda, *J. Plasma Phys.* **17**, 337 (1977).
- ¹⁸H. Baty, E. R. Priest, and T. G. Forbes, *Phys. Plasmas* **13**, 022312 (2006).
- ¹⁹M. Ottaviani and F. Porcelli, *Phys. Rev. Lett.* **71**, 3802 (1993).
- ²⁰D. Grasso, F. Califano, F. Pegoraro, and F. Porcelli, *Plasma Phys. Rep.* **26**, 512 (2000).
- ²¹N. F. Loureiro and G. W. Hammett, *J. Comput. Phys.* **227**, 4518 (2008).
- ²²L. Comisso, D. Grasso, F. L. Waelbroeck, and D. Borgogno, *Phys. Plasmas* **20**, 092118 (2013).
- ²³L. Chacón, A. N. Simakov, and A. Zocco, *Phys. Rev. Lett.* **99**, 235001 (2007).
- ²⁴A. Zocco, L. Chacón, and A. N. Simakov, *Phys. Plasmas* **16**, 110703 (2009).
- ²⁵A. N. Simakov and L. Chacón, *Phys. Rev. Lett.* **101**, 105003 (2008).
- ²⁶A. N. Simakov and L. Chacón, *Phys. Plasmas* **16**, 055701 (2009).
- ²⁷N. F. Loureiro, A. A. Schekochihin, and A. Zocco, *Phys. Rev. Lett.* **111**, 025002 (2013).
- ²⁸T. J. Schep, F. Pegoraro, and B. N. Kuvshinov, *Phys. Plasmas* **1**, 2843 (1994).
- ²⁹E. Cafaro, D. Grasso, F. Pegoraro, F. Porcelli, and A. Saluzzi, *Phys. Rev. Lett.* **80**, 4430 (1998).
- ³⁰S. I. Braginskii, *Reviews of Plasma Physics* **1**, 205 (1965).
- ³¹D. Grasso, F. Pegoraro, F. Porcelli, and F. Califano, *Plasma Phys. Control. Fusion* **41**, 1497 (1999).
- ³²L. Chacón and A. Stanier, “Fully implicit solution of the low- β extended MHD model,” (2015), In Preparation.
- ³³L. Chacón, D. A. Knoll, and J. M. Finn, *J. Comput. Phys.* **178**, 15 (2002).
- ³⁴L. Chacón and D. A. Knoll, *J. Comput. Phys.* **188**, 573 (2003).
- ³⁵D. A. Knoll and L. Chacón, *Phys. Rev. Lett.* **96**, 135001 (2006).
- ³⁶K. J. Bowers, B. J. Albright, L. Yin, W. Daughton, V. Roytershteyn, B. Bergen, and T. J. T. Kwan, *J. Phys.: Conf. Ser.* **180**, 012055 (2009).
- ³⁷Additional VPIC specific parameters: mass-ratio $m_i/m_e = 15.2$, guide field to reconnecting field ratio $B_g = 17.4$, electron thermal speed to speed of light ratio $v_{th,e}/c = 0.25$, electron plasma frequency to gyrofrequency ratio $\omega_{pe}/\Omega_{ce} = 2.5$, ion to electron temperature ratio $T_i/T_e = 1/4$. We find that the rate is insensitive to the precise values chosen (in particular, it is the same for a higher mass-ratio of 60.8), provided the two-field model parameters ρ_s and d_e are unchanged.
- ³⁸For the VPIC parameters used, the strong-guide field causes the Alfvén wave to be relativistic. Here we use the correct relativistic Alfvén speed to normalise the PIC rates, see [12].
- ³⁹A. N. Simakov, L. Chacón, and D. A. Knoll, *Phys. Plasmas* **13**, 082103 (2006).
- ⁴⁰Y.-M. Huang, A. Bhattacharjee, and T. G. Forbes, *Phys. Plasmas* **20**, 082131 (2013).

